Relaxation of geometrical frustration in NbSe₃ topological crystals

T. Tsuneta[*]

Graduate School of Education, Nara University of Education, Nara 630-8528, Japan

K. Yamamoto, N. Ikeda, and Y. Nogami

Graduate School of Natural Science and Technology, Okayama University, Okayama 700-8530, Japan

T. Matsuura and S. Tanda

Department of Applied Physics, Hokkaido University, Sapporo 060-8628, Japan

Here we report the structural study of NbSe₃ topological crystals via synchrotron x-ray measurements on individual microcrystals. Topological crystals are characterized by the shape of a ring or a twisted loop, thereby representing a translational and orientational order confined in topologically nontrivial, curved geometries. The crystal lattice of topological crystals is under considerable amount of strain. The volume-averaged strain asymptotically increases with thickness and curvature of a crystal. We present a structural model in which a ring crystal is composed of well-ordered domains in the shape of concentric cylinders. The internal structure reflects periodic accumulation and release of strain during the growth.

PACS number(s): 61.72.Bb, 61.72.Hh, 71.45.Lr

I. INTRODUCTION

Recently, we have demonstrated that transition-metal trichalcogenide (MX_3, M=Nb or Ta and X=S or Se), a group of fibrous and pliable materials, can grow as a microcrystal in the shape of a ring, Möbius strip,[1] and Hopf link.[2] Termed "topological crystals," they are the solid-state manifestation of topologically nontrivial geometries. Owing to their one-dimensional nature, MX_3 offer higher structural freedom than previously known two-dimensional materials, e.g., fullerenes[3,4] (sphere) and nanotubes[5] (cylinder).

Topological crystals intrigued many with unexplored physics in multiconnected geometries.[6–9] A particularly interesting feature of MX_3 topological crystals is their charge density wave (CDW),[10,11] a macroscopic quantum state. CDW emerges as a periodic modulation of electron-density coupled to ionic displacement. Mechanical deformations can affect its phase order, e.g., in a manner analogous to a superconductor under a magnetic field.[12] In fact, a series of experiments and simulations have revealed that CDW confined in the ring geometry has weakened intermolecular chain ordering. Namely, an enhancement of Ginzburg-Landau fluctuations,[13–15] a lowering of CDW pinning potential,[16] and higher damping time of phason excitations[17] in NbSe₃ topological crystals are reported. A unified understanding of these phenomena is still lacking.

However, little is known about how a topological crystal retains its crystal order against geometrical frustration. Suppose a crystalline order native to the Euclidean $\boldsymbol{R}^3$ is confined in a cylindrical space $\boldsymbol{R}^2 \times \boldsymbol{S}^1$. As the flat space cannot be mapped to the curved space isometrically and conformally at the same time, the translational and rotational order would acquire increasing strain depending on the position. In such a frustrated system, the original order may partially break into a new, unfrustrated structure.[18,19] Alternatively, it may develop a defect substructure characterized by periodic accumulation and release of strain as in Frank-Kasper metals[20,21] and liquid crystal blue phases.[22,23] These orders are known to perfectly fit curved space but when confined in a flat space, they develop characteristic disclination networks. NbSe₃ topological crystal is rare self-organized curved crystal that originally fits a flat space. And hence its structure and defect substructure is an interesting problem. In this paper, we report the structural study of individual, pristine topological crystals.

II. EXPERIMENT

NbSe₃ belongs to space group $P2_1/m$ with lattice parameters, a=10.009, b=3.4805, c=15.629 Å, and β=109.47°.[24] The crystal structure is composed of infinitely long, one-dimensional molecular chains aligned in the crystallographic b, which coincides with the circumference of topological crystals. The chains are bonded to each other in an anisotropic manner, forming stronger ionic/covalent bonding in c and weaker van der Waals bonding in a.[25] Consequently, NbSe₃ usually forms a thin whisker crystal.

Our samples fall into three categories: whisker, ring (more specifically, cylinder), and "figure-eight" strip, which is a loop with a twist of 2π on circling around the circumference. Figures 1(a) and 1(b) shows typical samples. See Ref. 26 for sample growth conditions. Figure 1(c) illustrates the coordi-
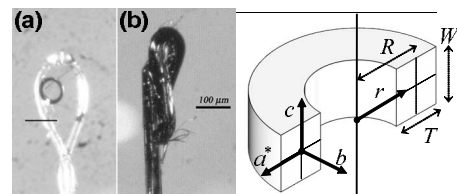
FIG. 1. Typical topological crystal samples: (a) ring and (b) figure-eight strip. Scale bars: 100 μm. (c) Crystallographic axes a^*, b, and c, and apparent size parameters radius R, thickness T, and width W. r, θ, and z of the cylindrical coordinates are parallel to a^*, b, and c, respectively.
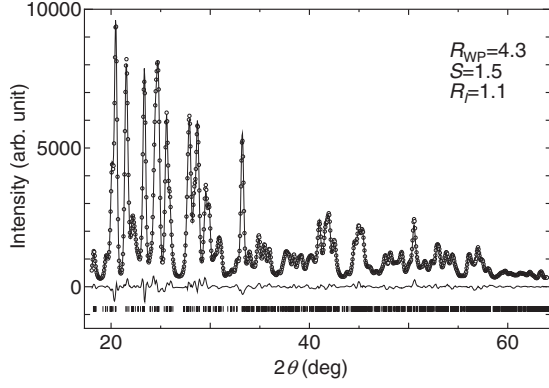
FIG. 2. A Rietveld analysis on a ring sample with $T/R=0.19$. The marks and the overlapping curve represent observed and calculated intensity, respectively. The difference between them is plotted below. Ticks are expected peak positions. The agreement factors are included in the figure.

nate system and three shape parameters: thickness T, radius R, which is defined at the middle of the thickness, and width W. Cylindrical coordinate axes r, θ, and z correspond to crystallographic axes a^*, b, and c, respectively.

We performed x-ray diffraction measurements employing synchrotron radiation at beam line BL02B1 of SPring-8. We could obtain intensity 10^{10} photons/s at the maximum, which is enough for our samples as small as ~ 10 μm $\times 50$ μm $\times 50$ μm. The beam is monochromatized to $\lambda = 0.9917$–0.9934 Å. A specially designed Gandolfi camera[27] is used to simulate powder diffraction photographs. Intensity is collected using an imaging plate and integrated into intensity vs 2θ data.

Structural refinement was carried out by the Rietveld analysis.[28] The peak-shape, prefered orientation, absorption, background, zero-point, scale, lattice, and crystal structural parameters were refined using RIETAN-2000 (Ref. 29) software. The peak shape is assumed to be a pseudo-Voigt function. Also it is assumed that the atomic occupancy is 1 and the isotropic atom displacement parameter is common among an atomic species. Figure 2 shows a Rietveld analysis. Agreement factors were typically as good as $S=1.5$, $R_{WP}=4.3$, and $R_I=1.1$ The lattice parameters of a single crystal whisker were determined as $a=10.008(2)$, $b=3.4860(7)$, $c=15.632(4)$ Å, and $\beta=109.45(1)°$. Only b has a non-negligible deviation of 0.16% from the measurement of pow-
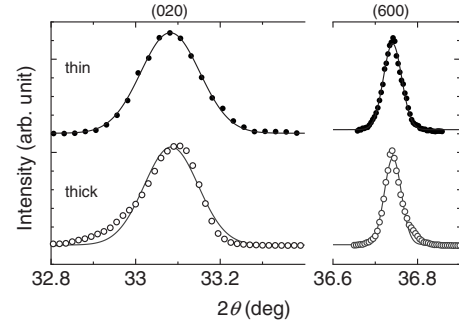
FIG. 3. Diffraction profiles of (020) and (600) peaks, for thin $T/R=0.19$ (upper) and thick $T/R=2.0$ (lower) rings. Curves show Gaussian fits.

dered sample.[24] This strain is presumably caused when the whisker sample is cut off. This gives an upper limit of the uncertainty of our pseudopowder diffraction method.

Further analyses of diffraction profiles are conducted for two of the ring samples. Isolated diffraction peaks are measured using a four-circle diffractometer and fitted to Gaussian curves, as shown in Fig. 3. The broadening of peaks is measured by half widths at half maximum C. C includes contributions from two factors, nonuniform lattice strain and finite size of domains of coherent diffraction. They are separated by the Williamson and Hall's method[30] in which the root-mean square of strain distributions $\Delta\varepsilon_i$ $(i=a,b,c)$ and the mean domain size l_i are related to C as

$$\frac{C \cos\theta}{\lambda} = \frac{K}{l_i} + \frac{2\Delta\varepsilon_i \sin\theta}{\lambda}, \tag{1}$$

where θ is the Bragg angle and K is the Scherrer constant. We set $K=1.0$. $C \cos\theta/\lambda$ would be a linear function of $\sin\theta/\lambda$, whose slope and intersect correspond to $2\Delta\varepsilon_i$ and $\frac{1}{l_i}$, respectively.

III. RESULTS

The lattice parameters of a topological crystal turned out under certain measure of strain. Volume-averaged lattice strain $\overline{\varepsilon_i}$ (an overline denotes an average) is defined with reference to lattice parameters in Ref. 24. Obtained $\overline{\varepsilon_i}$ are plotted in Fig. 4(a) (marks). Although the data are highly scattered in b, they have a tendency to contract in a while
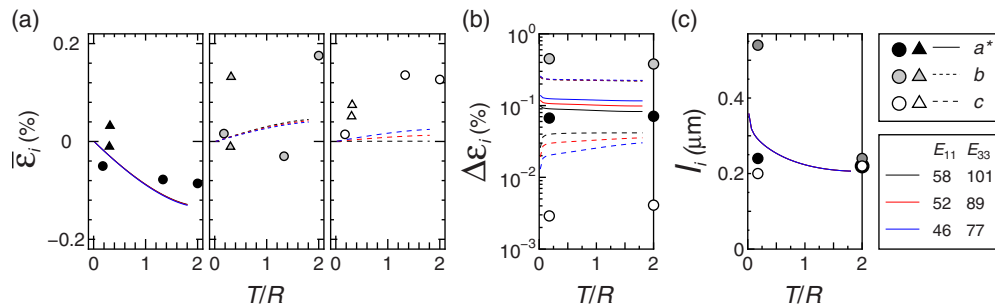
FIG. 4. (Color online) (a) Volume-averaged lattice strain $\overline{\varepsilon_i}$ $(i=a,b,c)$ plotted against a shape parameter T/R. (b) Root-mean-squared strain $\Delta\varepsilon$ and (c) mean size of coherent domains l_i of two ring samples. Circles and triangles represent ring and figure eight, respectively. Curves show data calculated for different elastic moduli.
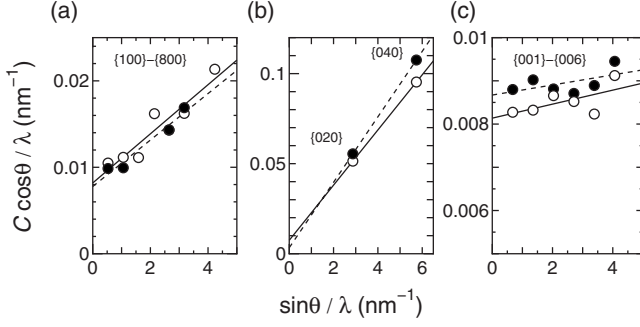
FIG. 5. The Williamson-Hall plots for diffraction series (a) {h00}, (b) {0k0}, and (c) {00l}. Filled and open circles represent peak profiles while dashed and solid lines represent linear fits, of the thin and thick samples, respectively.

expanding in b and c, monotonously depending on T/R. Strain in ring and figure-eight samples is alike. Besides, no lowering of the crystal symmetry is observed. The existence of 2_1 screw axis is confirmed by the intensity $I_{(020)}/I_{(040)} > 10^4$ for rings and $I_{(020)}/I_{(040)} > 10^3$ for figure-eight strips.

According to peak profile analyses, $\Delta\varepsilon_i$ has weaker T/R dependence. Figure 5 shows reasonably linear Williamson-Hall plots for selected diffraction series: (a) {h00}, (b) {0k0}, and (c) {00l}. Obtained $\Delta\varepsilon_i$ are exhibited in Fig. 4(b). While the magnitude of $\overline{\varepsilon_i}$ in each direction is alike, $\Delta\varepsilon_i$ in ring samples are highly anisotropic ($\Delta\varepsilon_b : \Delta\varepsilon_a : \Delta\varepsilon_c \sim 100 : 20 : 1$) and largest in the chain direction b. As plotted in Fig. 4(c), mean size of coherent domains are estimated at roughly 0.2 μm for the interchain directions while it is larger in the chain direction. These estimations give the lower limit of l_i since peak broadening for 0.2–0.4 μm is similar to broadening originating from the measurement apparatus.

IV. DISCUSSION

Let us evaluate lattice strain for the case with an elastic continuum body. Here we consider a rectangular material, $T \times 2\pi R \times W$ in dimensions, bent into a ring. The three principal axes of strain should coincide with the cylindrical coordinate axes of the ring. It is inferred that orthogonal crystallographic axes of NbSe$_3$, b, c, and a^*, take on them in an actual crystal. For the sake of simplicity, hereafter we treat NbSe$_3$ as an orthorhombic material with these axes as the coordinate axes.

Obviously, it is unrealistic that a ring crystal remains perfectly elastic. Assuming that the rotational symmetry is re-

tained so that the deformation is pure bending, an elastic ring undergoes stress

$$\sigma_b(r) = E_{22}\frac{r-R}{R}, \quad \sigma_a = \sigma_c = 0, \quad (2)$$

as a functions of r. Corresponding strain is given by

$$\varepsilon_b(r) = \frac{r-R}{R}, \quad \varepsilon_a = -\nu_{21}\varepsilon_b, \quad \varepsilon_c = -\nu_{23}\varepsilon_b. \quad (3)$$

E_{ii} ($i=1-3$) and ν_{ij} ($j=1-3$, $i \neq j$) represent anisotropic Young's moduli and Poisson's ratios, respectively. According to these equations, stress would be as large as 10 GPa even for our thinnest sample ($t/R=0.19$), far exceeding yield stress of usual matters. Moreover, volume-averaged strain in any direction would be zero in contrast to actual data.

Figure 6 describes a growth model of a ring crystal incorporating the generation of dislocations. (a) A beam of NbSe$_3$ crystal is bent into a ring. Here it should be remarked that a ring crystal tends to grow inward.[26] (b) The growth front at the inner surface is always under contractive stress. However, while the crystal is defect free, it can outwardly expand so that the strain profile remains symmetric as Eq. (2). (c) When local strain $|\varepsilon_b|$ reaches to an elastic limit k at the inner surface, the crystal yields. Dislocations with Burger's vector [010] are introduced to relax local strain down to $\varepsilon_b = \alpha k$ ($0 \leq \alpha < 1$). We assume $\alpha = 0$ (total relaxation) for the time being. Dislocations stay on the same atomic layer because the putative glide plane b-c is normal to the radius. In effect, the array of dislocations makes a domain wall between two defect-free cylindrical shells. (d) The subsequent growth accumulates contractive strain again, and the inner shell expands while the outer shell presses back. (e) The two shells attain an equilibrium position depending on their thickness. When the maximum strain at the growth front reaches to k again, the process repeats itself.

Now let us estimate strain distribution in this model. Total strain is given by the linear sum

$$\varepsilon_i = \varepsilon_i' + \varepsilon_i'', \quad (4)$$

where ε_i' and ε_i'' are contributions from bending and interlayer pressing, respectively.

ε_i' would not be as simple as the pure bending solution [Eq. (3)]. While the solution predicts that the ratio of Poisson strain would be $\Delta\varepsilon_a/\Delta\varepsilon_c = \nu_{21}/\nu_{23} \sim 1$, it is as large as 14 in actual samples. It is probably because the pure bending solution implies that a-c cross sections are deformed into a
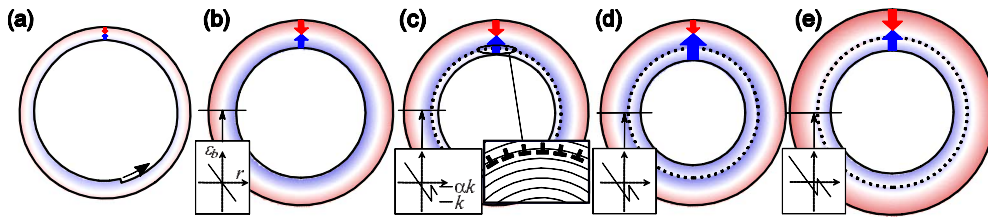
FIG. 6. (Color online) A growth model of a ring crystal. The color density indicates the magnitude of the strain, which is contractive in the inner half and expansive in the outer half. Small insets in (b)–(e) are strain profiles as a function of r. The other inset in (c) illustrates a domain boundary composed of dislocations formed on one of atomic layers (solid lines).
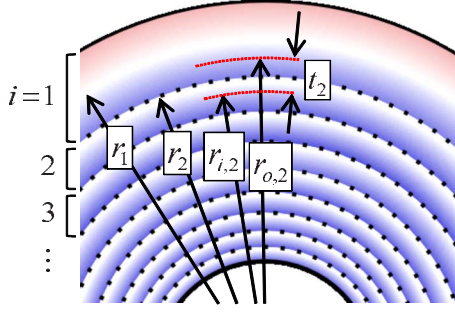
FIG. 7. (Color online) Geometrical configuration of a ring crystal composed of concentric cylindrical domains. $r_{i,n}$ and $r_{o,n}$ are the inner and outer radii with no external force applied, which does not necessarily coincide with actual radii. r_n and t_n are the radius of neutral plane and the neutral thickness, respectively.

bent rectangle. It causes mismatch at the boundary between cylindrical shells involving [001] dislocations. However, it is presumed that ε_b' reaches to the elastic limit before ε_c' and thus [010] dislocations dominate over [001]. Thereby ε_b' abruptly changes at the boundaries while ε_c' should remain continuous. We adopt the simplest bending deformation that ensures the continuity of ε_c', namely,

$$\varepsilon_{a,n}'(r) = -(\nu_{21} + \nu_{23}\nu_{31})\frac{r - r_n}{r_n},$$

$$\varepsilon_{b,n}'(r) = (1 - \nu_{23}\nu_{32})\frac{r - r_n}{r_n},$$

$$\varepsilon_{c,n}' = 0, \tag{5}$$

where r_n represent the radius of the neutral plane of the nth layer.

Stress due to interlayer pressing is determined by the distribution of the neutral thickness and radius of each layer. Figure 7 illustrates a ring crystal composed of N cylindrical shells. The size of the nth shell is defined by its outer and inner radii with no external force applied, $r_{o,n}$ and $r_{i,n}$, respectively. Its neutral plane is then at $r_n = (r_{o,n} + r_{i,n})/2$. The neutral thickness is given by $t_n = r_{o,n} - r_{i,n}$. Stress within the nth shell is expressed as[31]

$$\sigma_{a,n}''(r) = A_n(r)p_{n-1} + B_n(r)p_n,$$

$$\sigma_{b,n}''(r) = C_n(r)p_{n-1} + D_n(r)p_n, \tag{6}$$

and $\sigma_{c,n}'' = 0$, where

$$A_n(r) = \frac{r_{o,n}^2}{r^2}\left(\frac{r_{i,n}^2 - r^2}{r_{o,n}^2 - r_{i,n}^2}\right),$$

$$B_n(r) = -\frac{r_{i,n}^2}{r^2}\left(\frac{r_{o,n}^2 - r^2}{r_{o,n}^2 - r_{i,n}^2}\right),$$

$$C_n(r) = -\frac{r_{o,n}^2}{r^2}\left(\frac{r_{i,n}^2 + r^2}{r_{o,n}^2 - r_{i,n}^2}\right),$$

$$D_n(r) = \frac{r_{i,n}^2}{r^2}\left(\frac{r_{o,n}^2 + r^2}{r_{o,n}^2 - r_{i,n}^2}\right). \tag{7}$$

p_n represents the radial stress component at the interface between the nth and the $(n+1)$th shells, i.e.,

$$p_n = \sigma_{a,n}''(r_{i,n}) = \sigma_{a,n+1}''(r_{o,n+1}). \tag{8}$$

Strain is then obtained as

$$\varepsilon_{a,n}''(r) = \frac{1}{E_{11}}\sigma_{a,n}''(r) - \frac{\nu_{21}}{E_{22}}\sigma_{b,n}''(r). \tag{9}$$

Radial displacement $u_n(r)$ is derived as

$$u_n(r) = r_n\varepsilon_{b,n}''(r), \tag{10}$$

a linear combination of p_{n-1} and p_n.

Once the distribution of $r_{o,n}$ and $r_{i,n}$ $(n=1,\ldots,N)$ is determined, the condition of continuity of the interface position

$$r_{i,n} + u_n(r_{i,n}) = r_{o,n+1} + u_{n+1}(r_{o,n+1}) \tag{11}$$

provides linear simultaneous equations that are solved for p_n $(n=1,2,\ldots,N-1)$. Note that no external stress is applied at the surface, i.e., $p_0 = p_N = 0$. Then we can calculate stress and strain from a full set of p_n.

We run a numerical simulation of the growth process. Starting from a thin elastic layer having a neutral radius $r_1 = 40$ μm, we increased the thickness of the innermost layer by small steps, e.g., by one atomic layer ($\sim$Å). An addition of thickness dt increases $r_{i,n}$ and $r_{o,n}$ by $dt/2$, respectively. The growth of a layer stops when $|\varepsilon_b' + \varepsilon_b''|$ reaches to k at the inner surface and the next $(n+1)$th layer is formed. Local strain in the $(n+1)$th layer is relaxed to zero, i.e., its neutral plane coincides with the interface such as

$$r_{n+1} = r_{i,n} + u_n(r_{i,n}). \tag{12}$$

At the emergence of each layer, we computed the volume average of layer thickness and strain, and standard deviation of strain by Simpson's rule. They correspond to l_a, $\overline{\varepsilon_i}$, and $\Delta\varepsilon_i$, respectively.

Our simulation depends on six uncertain elastic moduli E_{ii} and ν_{ij} but few of them are arbitrary. The Young's modulus along the chain axis of MX_3 varies in the range of 100–300 GPa depending on measurement technique: an average of 350 GPa (Ref. 32) for NbSe$_3$, 100 GPa (Ref. 33), and 350 GPa (Ref. 34) for TaS$_3$, and 200 GPa (Ref. 35) for ZrTe$_3$. Here we adopt $E_{22} = 200$ GPa. Three additional moduli are determined from the linear isothermal compressibility of NbSe$_3$,[36] $K_a = 1.4\%/\text{GPa}$, $K_b = 0.13\%/\text{GPa}$, $K_c = 0.59\%/\text{GPa}$, and $K_\beta = -0.17\%/\text{GPa}$, according to

$$K_i = \frac{1}{E_{ii}} + \sum_{j \neq i}\frac{\nu_{ij}}{E_{jj}}. \tag{13}$$

Further, the moduli must be narrowed down in order to give physically meaningful Poisson's ratio. If we assume $0.05 < \nu_{ij} < 0.45$, only remaining arbitrary parameters are $E_{11} = 52 \pm 6$ and $E_{33} = 2.8E_{11} - 58 \pm 5$ GPa.

The results of calculations are plotted in Fig. 4 for $k = 0.44\%$ (arbitrarily chosen) and several combinations of E_{11} and E_{33}. Better fits are given by more anisotropic combina-

tions, e.g., $E_{11}=46$, $E_{22}=200$, and $E_{33}=77$ GPa, implying that the chain axis is three to five times harder than the others. This magnitude of anisotropy agrees with that of thermal expansion of NbSe$_3$.[24] The results reproduce overall qualitative features, namely, the sign and the order of magnitude of $\overline{\varepsilon_i}$ and the flatness and anisotropy of $\Delta\varepsilon_i$. The difference between experiments and calculations is ascribed to oversimplification as well as the uncertainty of elastic moduli. For example, a local change in growth conditions or the stochastic nature of grain boundary formation may disturb the balance of interlayer pressing, resulting in scattered $\overline{\varepsilon_b}$. In any case, the major contribution of $\overline{\varepsilon_a}$ is ε_a'' and it is always contractive since it originates from interlayer pressure.

Our result clearly suggests the existence of cylinder-shaped domains bounded by dislocation walls. Dislocation walls hamper a ring crystal from expanding so that the volume average of strain is relaxed to zero. The observed features, namely, nonzero $\overline{\varepsilon_i}$ and highly anisotropic $\Delta\varepsilon_i$, are the result of this.

An alternative possibility is that dislocations freely penetrate into a ring to negate local bending strain. If that is the case, however, both $\overline{\varepsilon_i}$ and $\Delta\varepsilon_i$ would have been far smaller. In fact, our calculations show that $\overline{\varepsilon_i}$ and $\Delta\varepsilon_i$ asymptotically approach zero when elastic limit strain tends to zero, or $k \rightarrow 0$, as in Fig. 8(a). Although quantitative evaluation is difficult, k should be no less than $\sim 0.1\%$, corresponding to a reasonable magnitude of yield stress, ~ 100 MPa.

At the other extreme, dislocations may be more sparse. When the growth front yields, not necessarily totally relaxation occurs because of interdislocation repulsion. This is expressed by $0 < \alpha < 1$ instead of $\alpha = 0$ and thus

$$r_{n+1} = \frac{r_{i,n} + u_n(r_{i,n})}{1 + \alpha k} \qquad (14)$$

instead of Eq. (12). At the limit as $\alpha \rightarrow 1$, every atomic layer has few dislocations and the relaxation of local strain is incomplete. A ring crystal would have higher interlayer pressure in the inner half, resulting in larger $\overline{\varepsilon_i}$. In fact, as shown in Fig. 8(b), $\alpha \neq 0$ results in greater $\overline{\varepsilon_i}$. Also since the inter-
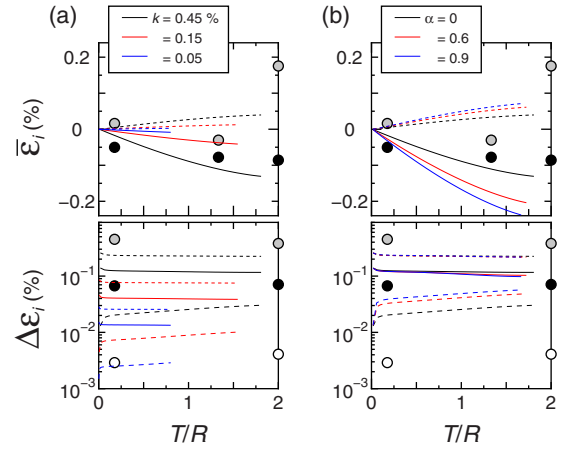
FIG. 8. (Color online) $\overline{\varepsilon_i}$ $(i=a,b)$ and $\Delta\varepsilon_i$ $(i=a,b,c)$. Curves are calculations for $E_{11}=46$, $E_{22}=200$, $E_{33}=77$ GPa and (a) $\alpha=0$ and varying k, (b) $k=0.45\%$ and varying α. Symbols represent measured values.

layer pressure is the main source of ε_c, $\Delta\varepsilon_c$ increases. It affects in the opposite direction to the stark anisotropy in $\Delta\varepsilon_i$ in the measured data. Again, although quantitative evaluation is difficult, the extreme case $\alpha \rightarrow 1$ would be ruled out.

In summary, we proposed that a ring crystal is composed of well-ordered domains in the shape of concentric cylinders, which are divided by walls of dislocations. This should be one typical aspect when a translational and orientational order is confined in a curved geometry. Possibly, the enhanced CDW fluctuations in topological crystals are related to the domain structure. We left the figure-eight geometry for future studies since its beyond the present approach.

ACKNOWLEDGMENTS

*tsuneta@nara-edu.ac.jp

[1] S. Tanda, T. Tsuneta, Y. Okajima, K. Inagaki, K. Yamaya, and N. Hatakenaka, Nature (London) **417**, 397 (2002).

[2] T. Matsuura, M. Yamanaka, N. Hatakenaka, T. Matsuyama, and S. Tanda, J. Cryst. Growth **297**, 157 (2006).

[3] R. Tenne, J. Mater. Res. **21**, 2726 (2006).

[4] H. Kroto, J. Heath, S. Obrien, R. Curl, and R. Smalley, Nature (London) **318**, 162 (1985).

[5] S. Iijima, Nature (London) **354**, 56 (1991).

[6] K. Yakubo, Y. Avishai, and D. Cohen, Phys. Rev. B **67**, 125319 (2003).

[7] M. Hayashi, H. Ebisawa, and K. Kuboki, Phys. Rev. B **72**, 024505 (2005).

[8] K. Harigaya, A. Yamashiro, Y. Shimoi, and K. Wakabayashi, Synth. Met. **152**, 261 (2005).

[9] Y. Asano, Phys. Rev. B **72**, 092508 (2005).

[10] K. Tsutsumi, T. Takagaki, M. Yamamoto, Y. Shiozaki, M. Ido, T. Sambongi, K. Yamaya, and Y. Abe, Phys. Rev. Lett. **39**, 1675 (1977).

[11] R. M. Fleming, D. E. Moncton, and D. B. McWhan, Phys. Rev. B **18**, 5560 (1978).

[12] M. Hayashi, H. Ebisawa, and K. Kuboki, Phys. Rev. B **76**, 014303 (2007).

[13] T. Tsuneta, S. Tanda, K. Inagaki, Y. Okajima, and K. Yamaya, Physica B **329-333**, 1544 (2003).

[14] K. Shimatake, Y. Toda, and S. Tanda, Phys. Rev. B **73**, 153403 (2006).

[15] T. Nogawa and K. Nemoto, Phys. Rev. B **73**, 184504 (2006).

[16] T. Matsuura, T. Tsuneta, K. Inagaki, and S. Tanda, Phys. Rev. B **73**, 165118 (2006).

[17] T. Matsuura, K. Inagaki, and S. Tanda, Phys. Rev. B **79**, 014304 (2009).

[18] M. Kléman, Adv. Phys. **38**, 605 (1989).

[19] R. Mosseri, C. R. Chimie **11**, 192 (2008).

[20] F. C. Frank and J. Kasper, Acta Crystallogr. **11**, 184 (1958).

[21] D. R. Nelson, Phys. Rev. B **28**, 5515 (1983).

[22] S. Meiboom, M. Sammon, and W. F. Brinkman, Phys. Rev. A **27**, 438 (1983).

[23] S. Meiboom, M. Sammon, and D. W. Berreman, Phys. Rev. A **28**, 3553 (1983).

[24] J. L. Hodeau, M. Marezio, C. Roucau, R. Ayroles, A. Meerschaut, J. Rouxel, and P. Monceau, J. Phys. C **11**, 4117 (1978).

[25] J. A. Wilson, Phys. Rev. B **19**, 6456 (1979).

[26] T. Tsuneta and S. Tanda, J. Cryst. Growth **264**, 223 (2004).

[27] Detailed description will be published elsewhere.

[28] H. M. Rietveld, J. Appl. Crystallogr. **2**, 65 (1969).

[29] F. Izumi and T. Ikeda, Mater. Sci. Forum **321-324**, 198 (2000).

[30] G. Williamson and W. Hall, Acta Metall. **1**, 22 (1953).

[31] G. Lamé, *Leçons sur la Théorie de l'Élasticité* (Gauthier-Villars, Paris, 1852).

[32] J. W. Brill and N. P. Ong, Solid State Commun. **25**, 1075 (1978).

[33] T. M. Tritt, M. J. Skove, and A. C. Ehrlich, Phys. Rev. B **43**, 9972 (1991).

[34] J. W. Brill, Solid State Commun. **41**, 925 (1982).

[35] T. N. O'Neal, J. W. Brill, B. Ganguly, X.-D. Xiang, and G. Minton, Synth. Met. **31**, 215 (1989).

[36] K. Yamaya and G. Oomi, J. Phys. Soc. Jpn. **52**, 1886 (1983).